Journal of Catalysis 284 (2011) 77–89

Contents lists available at SciVerse ScienceDirect

Journal of Catalysis

journal homepage: www.elsevier.com/locate/jcat

Ethanol steam reforming over Co-based catalysts: Investigation of cobalt coordination environment under reaction conditions

Burcu Bayram [a], I. Ilgaz Soykal [a], Dieter von Deak [a], Jeffrey T. Miller [b], Umit S. Ozkan [a,*]

[a] Department of Chemical and Biomolecular Engineering, The Ohio State University, 140 W. 19th Avenue, Columbus, OH 43210, United States
[b] Chemical Sciences and Engineering Division, Argonne National Laboratory, 9700 S. Cass Avenue, Argonne, IL 60439, United States

ARTICLE INFO

Article history:
Received 31 May 2011
Revised 30 August 2011
Accepted 1 September 2011
Available online 6 October 2011

Keywords:
X-ray absorption spectroscopy
XANES
EXAFS
In situ XRD
Ethanol steam reforming
Cobalt

ABSTRACT

The transformations and the state of cobalt species during steam reforming of ethanol over Co/CeO_2 were investigated using in situ X-ray diffraction, controlled-atmosphere X-ray absorption fine structure, and X-ray photoelectron spectroscopy as well as steady state activity measurements. The catalyst was pretreated under an oxidizing or reducing atmosphere prior to characterization and activity testing to yield a Co_3O_4-rich or a Co^0-rich surface, respectively. While Co_3O_4 was found to be inactive for ethanol steam reforming, gradual activation of the oxidation-pretreated catalyst with temperature through reduction in Co_3O_4 took place under reaction conditions, and, over the activated catalyst, a mixture of both CoO and metallic Co were observed. Over the reduction-pretreated catalyst, metallic Co was partially oxidized to CoO during steam reforming of ethanol. The extent of cobalt reduction was observed to be independent of the initial state of the metal on the catalyst surface, and cobalt phase had the same composition under reaction above 450 °C.

1. Introduction

With the increasing demand on renewable energy technologies that leave minimal carbon footprint, research efforts on the production of hydrogen from renewable sources such as bio-derived oxygenates have been gaining momentum. In addition to having high gravimetric energy density and being a potential fuel for fuel cells, which allow more efficient energy conversion, when produced from bio-derived liquids, use of hydrogen as the energy carrier has minimal environmental impact due to the potential of recycling the CO_2 produced in the process via photosynthesis during plant growth [1]. The low sulfur content of the bio-derived liquids is another environmental advantage. Ethanol has emerged as a promising bio-derived liquid and received significant research attention because of its low toxicity and ease of handling, and the possibility of producing it from a variety of feedstocks that would not interfere with food or feed supply, such as lignocellulosic material.

Catalytic steam reforming is a cost-effective and efficient technology for hydrogen production from ethanol. A large number of catalytic systems have been reported to exhibit activity for the ethanol steam reforming (ESR) reaction, and these systems have been in a number of recent reviews [2–4]. Aupretre et al. [5] compared the catalytic activities of noble-metal-based (Rh, Pt) and non-noble-metal-based (Cu, Ni, Zn, and Fe) catalysts for ESR. These authors reported Rh-based catalysts to possess superior catalytic activity in terms of both hydrogen yield and CO_2 selectivity. Similar studies in the literature have focused on noble-metal catalysts, such as Ru, Pd, Au, Re, Pt, Ir, and Rh [6–15] and reported high activities in a wide temperature and gas hourly space velocity range. Cobalt catalysts supported on a wide variety of metal oxide supports, such as zirconia, ceria, magnesia have shown promising ethanol steam reforming activities [16,17]; however, the nature of the cobalt active sites during the steam reforming reaction continues to be a topic of debate. Through ethanol, temperature-programmed desorption experiments carried out over a cobalt foil under ultra high vacuum conditions. Hyman and Vohs [18] showed that metallic cobalt sites were active in ethanol decarbonylation and Co^{2+} promoted dehydrogenation reactions to yield acetaldehyde species, while mostly complete oxidation products were observed over highly oxidized cobalt surfaces. The in situ magnetic characterization of cobalt during ethanol steam reforming over unsupported Co_3O_4 and metal oxide-supported cobalt catalysts was reported by Llorca et al. [19,20]. Over both types of catalysts, the authors observed the coexistence of an equilibrium state between reduced and oxidized phases of cobalt under reaction conditions. In a more recent study, Lin et al. [21] reported that the equilibrium state between CoO and Co^0 was governed by the feed stream composition as well as the catalyst pretreatment conditions. Similar results on the coexistence of Co^0 and CoO phases during ethanol steam reforming have been reported through in situ X-ray diffraction (XRD) studies on unsupported Co_3O_4 [22]. Batista

* Corresponding author. Fax: +1 614 292 3769.
E-mail address: ozkan.1@osu.edu (U.S. Ozkan).

0021-9517/$ - see front matter © 2011 Elsevier Inc. All rights reserved.
doi:10.1016/j.jcat.2011.09.001

et al. [23] reported that metallic cobalt sites constituted the active sites for ESR over cobalt-based catalysts. The metal–support interaction adds another level of complexity to the identification of active cobalt species for steam reforming of ethanol, and the nature of the ESR active sites remains as an important issue under debate.

Previously, through investigating the effect of a number different catalyst preparation methods and parameters, we have shown that strong metal–support interaction and high metal–support interface area were important factors that influence catalyst activity as well as stability [17,24–28]. The impregnation medium used for introducing the active metal onto the support [27] and the nature of cobalt precursor [24] was shown to play an important role in achieving high dispersion of cobalt species and thus, achieving high activity and stability over Co-based ethanol steam reforming catalysts. Novel catalyst synthesis techniques, namely solvothermal decomposition and reverse microemulsion, were also found to improve the catalyst activity by enhancing the intimate contact between the support and the active metal [28]. Furthermore, the nature of the support was found to play a key role in achieving high activity and stability by providing delivery of oxygen species to close proximity of ethoxy species and resulting in suppression of both sintering of cobalt and coke formation by enhancing oxidation of deposited carbon. In this context, ceria-based catalysts with significantly higher oxygen storage capacity and mobility were found to be highly active, selective, and stable for ethanol steam reforming [25]. Creation of oxygen vacancies through the introduction of a di-valent cation, such as Ca, resulted in further improvements in the hydrogen yields, turnover frequencies, and lower liquid by-products [26]. In this paper, we present results of in situ and/or controlled-atmosphere investigation of the transformation and the state of cobalt species on a Co/CeO_2 catalyst during steam reforming of ethanol. The effect of two different pretreatment procedures, namely oxidizing and reducing pretreatment conditions, on the coordination environment of cobalt was studied using in situ X-ray diffraction, controlled-atmosphere X-ray absorption fine structure spectroscopy, and X-ray photoelectron spectroscopy in addition to steady state performance evaluations on oxidation- and reduction-pretreated catalysts. Evolution of species on the surfaces of oxidized and pre-reduced catalysts was also examined through in situ diffuse reflectance infrared Fourier transform (DRIFT) spectroscopy. It should be noted that there was no attempt to control the ratio of Co-to-CoO phases in the catalytic systems. Instead, the study focused on examining the evolution of the phases as the catalyst was exposed to the reaction medium for a certain length of time at each temperature.

2. Experimental

2.1. Catalyst preparation

A Co/CeO_2 catalyst with 10 weight percentage nominal cobalt loading was prepared by a previously described incipient wetness impregnation route where commercial cerium (IV) oxide (Aldrich) is impregnated with an aqueous solution of cobalt (II) nitrate hexahydrate (Aldrich, 99.999%) [27]. Prior to impregnation, the ceria support was calcined at 550 °C for 3 h under air. Impregnation of cobalt on the support was carried out in five consecutive steps by drying the impregnated catalyst at 110 °C overnight in between impregnation steps to improve the homogeneity of the resulting catalyst. Following the final impregnation and drying step, the catalyst was calcined at 450 °C for 3 h under a flow of air.

2.2. Catalyst characterization

Surface area and pore volume measurements were obtained on a Micromeritics ASAP 2020 accelerated surface area and porosimetry instrument, using krypton adsorption/desorption isotherms collected at liquid nitrogen temperature. The desorption branch of the isotherm was used to determine the BJH pore size distributions. Before measurement, the catalyst was degassed for 12 h at 130 °C under a vacuum better than 2 μm Hg. Prior to the surface area analysis of the reduced catalyst, a reduction step was performed in situ, using the same procedure outlined above. Krypton physisorption measurements showed BET surface areas of the CeO_2 support, oxidized Co/CeO_2 and reduced Co/CeO_2 catalysts to be 9 m^2/g, 7 m^2/g, and 10 m^2/g, respectively, while pore size distributions were consistent with a mesoporous material with pore size distributions centered at 17 nm.

The dispersion measurements were obtained using N_2O chemisorption technique outlined earlier by Jensen et al. [29]. For these measurements, 200 mg of the catalyst was packed in a ¼″ OD fixed bed quartz reactor with a quartz frit and placed inside a fast-response furnace (Carbolite, MTF 10/15/130). The sample was reduced in situ at 400 °C using 5% H_2 in He for 2 h. The reactor was then flushed with He at the same temperature and cooled under helium. N_2O chemisorption was performed by introducing a stream of 3%N_2O/He to the reactor at 40 °C. Species in the m/z = 12 to m/z = 46 range were monitored via an online mass spectrometer (MKS – Cirrus II). The mass spectrometer was calibrated for instrumental sensitivity factors and the contribution of m/z = 28 fragment of N_2O to the m/z = 28 trace. Throughout the experiment, N_2O and N_2 were the only species detected in the reactor effluent. For quantification of the N_2 formation, known volumes of N_2 were injected to the mass spectrometer under the same flow conditions with a 250 ml sample loop connected to an automated six-port valve. The number of O atoms consumed is calculated through N_2 evolution, and the number of surface Co sites is calculated after the Fickian diffusion correction, assuming 1:1 Co/O ratio. Due to the low surface area of the support, the dispersion of Co on the ceria surface was low (~1%).

The temperature-programmed reduction profiles (H_2-TPR) of Co/CeO_2 catalysts were collected on an online mass spectrometer (Cirrus II, MKS Instruments, 1–300 amu) operated in the selective ion-detection mode. Both m/z = 2 and m/z = 18 signals were monitored. 0.1 g of catalyst sample was packed inside a ¼″ OD quartz U-tube reactor made of quartz using quartz wool plugs. The catalyst was pretreated in He at 400 °C for 30 min followed by cooling to room temperature in He. Then, 5% H_2/He (30 cm^2/min) was introduced to the reactor at room temperature, and the mass signals were allowed to stabilize for at least 30 min before ramping the temperature at 10 °C/min to 650 °C.

The in situ XRD patterns during ethanol steam reforming over Co/CeO_2 were collected on a Bruker D8 Advance X-ray diffractometer with monochromatic Cu Kα radiation (λ = 1.5418 Å) through a tube operated at 40 kV and 50 mA and equipped with an Anton Paar HTK1200 controlled-atmosphere oven prior to the collection of in situ XRD patterns, and the catalyst samples were subjected to either an oxidation or a reduction pretreatment. The oxidation pretreatment involved heating the catalyst at 400 °C under air (30 ccm) for 30 min, and samples subjected to this pretreatment will be denoted as Co/CeO_2(O). The pre-reduction step consisted of heating the catalyst to 400 °C under a flow of He (30 ccm) for 30 min followed by reduction for 2 h in 5% H_2/He (30 ccm) at the same temperature and purging with He (30 ccm) for 1 h at 450 °C. Samples subjected to this pretreatment will be denoted as Co/CeO_2(R).

The ethanol steam reforming mixture contained ethanol and water at a molar ratio of 1-to-10 and an ethanol concentration of 0.3%. An O_2 trap was installed in the UHP helium line (VICI Valco Instruments, HP2 heated helium purifier) to remove any oxygen impurity that might be present in helium before it reaches the reactor. Throughout the XRD experiments, a linear heating rate of

12 °C/min was used and the temperature was held constant at each temperature step for at least 30 min prior to the collection of the diffraction patterns. In order to investigate the progression of the reduction in cobalt oxide species, another experiment was conducted where an oxidized catalyst was directly put under the abovementioned reaction stream at 500 °C and in situ XRD patterns were collected as a function of time-on-stream. During these experiments, the in situ XRD patterns were collected at 1 h intervals for 12 h. The identification of the crystalline phases through the collected diffraction patterns was performed using the International Center for Diffraction Data (ICDD) database.

Controlled-atmosphere X-ray absorption fine structure (XAFS) data at the Co K-edge (7709 eV) were collected at the bending magnet beamline (5BM-D) of the Dow-Northwestern-DuPont Collaborative Access Team (DND-CAT) of the Advanced Photon Source, Argonne National Laboratories. The measurements were made in transmission mode with the Si(1 1 1) monochromator detuned by 30% to eliminate the higher order harmonics in the beam. The sample thickness was chosen to give an absorption edge jump of about 1.0 at the Co K-edge. The 10% Co/CeO_2 catalyst was mixed with SiO_2 at a ratio of 1:4 and finely ground (<150 mesh) to obtain a homogeneous mixture. Approximately 22 mg of the mixture was then pelletized in a 6-mm polished steel die and placed inside a 5-cm-long quartz tube (6.5 mm ID) and supported with quartz wool plugs. The sample was then centered in a 45×2 cm controlled-atmosphere XAFS chamber that was fitted with Kapton® windows. The XAFS reactor setup allowed continuous flow of the reactants as well as the isolation of the catalyst sample. Although contact geometry of the catalyst with the gases in the XAS experiments does not simulate a true plug flow reactor (as described in a recent article [30]), this cell configuration has been used in many other studies reported in the literature [31,32].

The catalyst in the controlled-atmosphere XAFS cell was pretreated following either one of the pretreatment procedures outlined above. Ethanol steam reforming reaction mixture contained 0.3% of ethanol and 3% H_2O. The XAFS data on the pretreated catalyst samples were collected following ethanol steam reforming at every 50 °C in the 350–500 °C region. At each temperature, the catalyst was kept onstream for 1 h before flushing the cell with helium (100 ccm) for 15 min. The catalyst was cooled to room temperature under the helium atmosphere and sealed under the same atmosphere for data collection. The XAFS data were collected at room temperature under helium. Helium (UHP) was further purified by an O_2 trap (VICI Valco Instruments, HP2 heated helium purifier) installed upstream of the reaction chamber. Following data collection, the cell was heated to the next temperature under helium and the steam reforming feed was introduced. WinXAS data analysis software package was used for analysis of the collected XAFS data following standard procedures outlined in [33]. Phase shifts and backscattering amplitudes used for the analysis of the data were obtained from the experimental reference spectra collected on reference compounds, i.e., CoO and Co-foil. XANES reference spectra were obtained for Co_3O_4, CoO, and Co-foil. The coordination parameters for Co—Co and Co—O—Co shells were obtained by the isolation of the respective shells from the EXAFS spectrum using the different method outlined earlier by Miller et al. [34]. The coordination numbers obtained through fitting the isolated shells are then divided by the fraction of that component obtained from XANES analysis for calculating the corrected coordination numbers. The large contribution from Co—Co shell did not allow isolation of the Co—O shell to obtain accurate coordination parameters.

Controlled-atmosphere X-ray photoelectron spectra of the Co/CeO_2 samples were collected in a Kratos AXIS Ultra X-ray photoelectron spectrometer, using monochromatized Al Kα (1486.7 eV) X-ray source operated at 13 kV and 10 mA. The surface chemical species of catalysts prepared as previously described were characterized before and after ethanol steam reforming reaction. The same reaction system as described in Section 2.3 for steady state catalytic activity testing was used to treat the catalysts. After the reaction treatment had concluded, the system was flushed with ultra-pure helium for 15 min at rate of 30 ccm. The vertical plug flow reactor was sealed and removed from the reaction system. The catalyst sample was then cast into a pellet and transferred to the transfer arm of the spectrometer in a nitrogen atmosphere. The charge neutralizer was operated at a current of 2.0 A and a filament bias of 1.3 V. A complete survey spectrum, as well as spectra for the regions for O 1s, C 1s, Co 2p, and Ce 3d was collected for each catalyst sample. Collected data were corrected for charge shifting using standard C 1s binding energy of 284.5 eV. XPS Peak 4.1 software package was used for curve fitting Spectra baselines were determined using Shirley-type background fitting. Spectra were deconvoluted using Lorentzian–Gaussian combination peaks.

In situ diffuse reflectance Fourier transform infrared spectroscopy (DRIFTS) experiments were performed using a Thermo NICOLET 6700 FTIR spectrometer equipped with a liquid nitrogen-cooled MCT detector and a KBr beam splitter. The in situ cell consisted of a Smart Collector™ controlled-atmosphere chamber with ZnSe windows. Similar to the abovementioned XRD experiment, the catalyst was oxidized or reduced in situ following one the pretreatment procedures outlined above prior to introducing the steam reforming feed to the controlled-atmosphere chamber. Following the aforementioned treatment step, the temperature was raised to 500 °C under helium flow and the background spectra were collected every 50 °C, during cooling. At 25 °C, another background spectrum was collected and the ethanol steam reforming feed with a water-to-ethanol molar ratio of 10:1 and 0.3% ethanol concentration was introduced to the DRIFTS chamber. The feed stream was obtained by flowing helium through two separate bubblers containing water and ethanol kept at room temperature. At each temperature, the reaction was allowed to progress for 30 min before collecting sample spectra while reactants are still flowing through the DRIFTS chamber. After the collection of the sample spectrum, the DRIFTS chamber was flushed with helium for 8 min and another sample spectrum was collected at the same temperature. Following the collection of this second spectrum, the temperature was increased under the reaction feed and the procedure was repeated at 50 °C intervals up to 500 °C. Any oxygen impurity in helium was removed by an O_2 trap (VICI VALCO Instruments, HP2 heated He purifier) prior to feeding the gas to the DRIFTS chamber.

2.3. Steady state catalytic activity testing

The steady state ethanol steam reforming activity data were collected in the 350–500 °C range using a fixed bed flow reactor setup using a 4-mm ID quartz reactor with a quartz frit. For each run, a 100 mg batch of the Co/CeO_2 catalyst was packed inside the reactor. The reactor was placed inside a resistively heated furnace (Carbolite, MTF 10/15/130), and the temperature was controlled by an Omega CSC232 PID temperature controller. Helium was used as the carrier gas, and the reactants were introduced to the helium stream using a heated evaporator and syringe pump assembly. The reactants, water, and ethanol, at a 10-to-1 M ratio, were fed to an evaporator maintained at 230 °C, using pulse-free syringe pumps (Cole-Parmer). The gas lines in contact with the reactant gas stream were heated to 130 °C to prevent condensation. For the reaction experiments, the feed stream to the reactor constituted of 0.8% ethanol and 8% water in helium at a WHSV of 2.7 g EtOH $(g\,cat)^{-1}\,h^{-1}$. The steady state reaction experiments were run in the kinetically controlled regime by maintaining the reaction conditions away from equilibrium at all temperatures

during the activity testing experiments. By using the Weisz–Prater criterion for internal diffusion effects and Mear's Criterion for external diffusion effects, it was verified that there were no transport limitations in the system. The reported reactant conversion and product yield values are representative of the catalytic activity after steady state was reached at each temperature. Prior to the catalytic activity tests, the catalyst samples were subjected to either an oxidation or a reduction pretreatment as outlined in Section 2.2.

The quantitative analysis of the reactor effluents was carried out by online gas chromatography (Shimadzu Scientific 2010) equipped with a Carboxen® column coupled with a pulsed discharge helium ionization detector (PDHID), which was used to separate and detect H_2, CO, and CO_2 and a Q-Bond column with a flame ionization detector (FID) to separate and detect the hydrocarbon species. The carbon balances were always better than 95%.

Average turnover frequency (TOF) for H_2 formation was defined as

$$\mathrm{TOF} = \frac{\text{moles of } H_2 \text{ produced/s}}{\text{moles of Co on the surface}}$$

TOFs were also calculated for the Co^0 and Co^{2+} sites individually. In these calculations, it was assumed that, at a given temperature, a Co^0 site had the same TOF whether it was in a pre-reduced catalyst matrix or not. The same assumption was used for the Co^{2+} sites. At each temperature, TOFs for the two sites (TOF^0_{co} and TOF^{2+}_{co}) were calculated using the following two equations:

$$(n_{Co^o})_O \times (TOF_{Co^o}) + (n_{Co^{2+}})_O \times (TOF_{Co^{2+}}) = (\text{molecules of } H_2 \text{ produced/s})_O$$

$$(n_{Co^o})_R \times (TOF_{Co^o}) + (n_{Co^{2+}})_R \times (TOF_{Co^{2+}}) = (\text{molecules of } H_2 \text{ produced/s})_R$$

where subscripts "O" and "R" refer to the catalysts that went through oxidation and reduction pretreatments, respectively. The terms n^0_{Co} and n^{2+}_{Co} represent the number of Co^0 and Co^{2+} sites, respectively, calculated from XANES data for each catalyst at each temperature.

3. Results and discussion

3.1. Temperature-programmed reduction

The reduction characteristics of the Co/CeO_2 catalyst were investigated by temperature-programmed reduction technique in the 50–650 °C range. The H_2 consumption profile as a function of temperature is presented in Fig. 1 together with deconvolution of the H_2 uptake profile for quantitative analysis. During the TPR experiment, H_2 uptake was observed as a well-resolved doublet in the 250–500 °C region and the doublet was curve-fitted with two symmetric peaks with maxima corresponding to 330 °C and 400 °C. Such a two component reduction profile for reduction of Co/CeO_2 has been previously reported [35] and is consistent with a stepwise reduction scheme, where the first consumption band is associated with reduction of Co_3O_4 to CoO while the second consumption band arises from reduction of CoO to metallic Co. There were no H_2 consumption features that could be associated with the onset of the reduction of the ceria support in the temperature range the TPR experiment was carried out. The assignment of the H_2 consumption bands was further verified by calculating the area under each fitted component. The area ratio of the second fitted component to the fist fitted component was calculated to be 3, which is in agreement with the stoichiometry of stepwise Co_3O_4 to CoO to Co^0 reduction and further verifies the peak assignments.

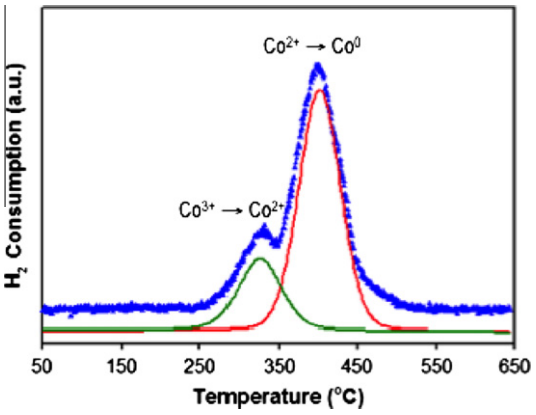

Fig. 1. Temperature-programmed reduction profile of Co/CeO_2.

3.2. In situ X-ray diffraction

The transformation of Co phases during steam reforming of ethanol at different temperatures over Co/CeO_2(O) and Co/CeO_2(R) catalysts was investigated using in situ XRD technique. Fig. 2 shows the in situ XRD patterns collected during ethanol steam reforming over Co/CeO_2(R). XRD patterns for the pristine and reduced catalysts are provided for comparison. The XRD pattern for the pristine catalyst was obtained at room temperature before the catalyst treatment. Three diffraction peaks at 2Θ values of 31°, 33°, and 37° were resolved over the pristine catalyst. The well-resolved peak at 33° corresponds to diffraction by [200] plane of CeO_2 in face-centered cubic cerianite structure (ICDD #34–394). The cerianite phase persists throughout the pretreatment and ESR stages, regardless of the conditions under which the catalyst was pretreated. Crystallite size calculations using Scherrer's method over the [200] plane of CeO_2 yielded an average ceria crystallite size of approximately 60 nm and did not show any changes in the crystallite size of this phase during ethanol steam reforming over this catalyst, regardless of the pretreatment conditions.

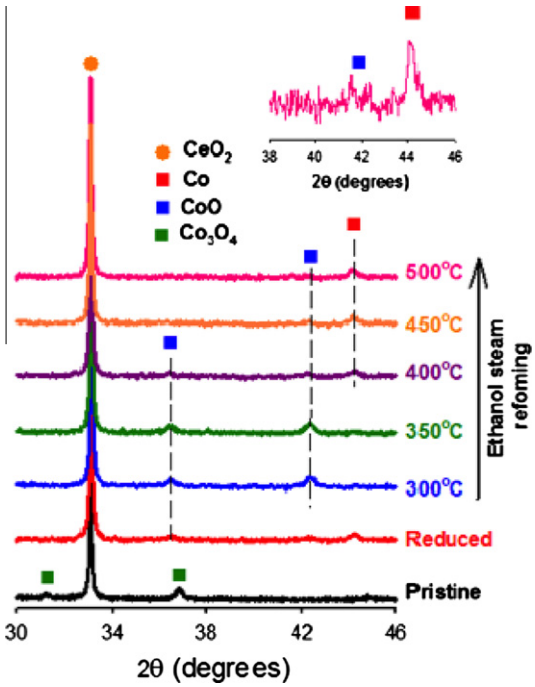

Fig. 2. In situ XRD patterns collected as a function of temperature during ethanol steam reforming over Co/CeO_2(R) (inset shows the Co/CeO_2(R) at 500 °C).

The remaining 31° and 37° peaks were associated with the [220] and [311] planes of Co_3O_4 (ICDD #42–1467). The XRD pattern for the catalyst after reduction pretreatment was obtained at room temperature under an inert flow. Following reduction treatment, the peaks associated with Co_3O_4 disappeared and the formation of a new diffraction peak at 44° together with two weakly resolved peaks at 36.5° and 42.4° was observed. The well-resolved peak located at 44° corresponds to the [111] plane of metallic cobalt (ICDD #15–806), while the 36.5° and 42.4° peaks were associated with the [111] and [200] planes of CoO (ICDD #43–1004). With the introduction of the reaction feed over Co/CeO_2(R) at 300 °C, a decrease in the intensity of the peak associated with metallic cobalt phase (44°) and a concomitant increase in the intensities of CoO peaks (36.5° and 42.4°) were observed. This observation suggests a partial re-oxidation of metallic cobalt species to CoO. The CoO phase persisted under reaction conditions at 350 °C, but further increase in the reaction temperature resulted in the reduction in CoO to form metallic cobalt species, as suggested by the decrease in the intensity of CoO diffraction peaks and increase in the 44° peak, which was associated with metallic cobalt. The in situ XRD pattern collected after 30 min on stream of ethanol steam reforming at 500 °C suggests that metallic Co is the major cobalt phase observed to exist together with the cerianite phase of CeO_2. Although very weak, the diffraction line that corresponds to the CoO phase still exists following reaction at 500 °C, as seen in the inset (Fig. 2).

As discussed above, re-oxidation of metallic cobalt on the pre-reduced catalyst was observed during ethanol steam reforming at 300 °C. One plausible explanation for this re-oxidation phenomenon is oxygen migration from the support to metallic cobalt moieties to result in cobalt oxide species. Labile oxygen species of the CeO_2 support play an important role in improving the activity and stability of Co-based steam reforming catalysts not only by suppressing coke formation, but also by promoting oxygen delivery to close proximity of ethoxy species to enable higher hydrogen yields [25]. Another plausible explanation is the re-oxidation of metallic cobalt moieties with oxygen from dissociative adsorption of water from the reaction mixture. Similar observations on the conversion of metallic Co-to-CoO under the reaction conditions have been previously reported [21,36], and the extent of the re-oxidation was found to be influenced by the ethanol-to-water ratio over a 10% Co/CeO_2—ZrO_2 catalyst [21].

With the aim of providing further insight into this phenomenon, a Co/CeO_2 catalyst was reduced under 5%H_2/He at 450 °C for 2 h and then, kept in helium atmosphere at the same temperature while XRD patterns were collected at one hour intervals after switching to the inert atmosphere. The reduction temperature used for this experiment was higher than the temperature used in pre-reduction procedure prior to reaction experiments. In agreement with the results discussed above, the XRD pattern collected immediately after switching to the inert atmosphere shows the presence of metallic Co phase (44°) together with the cerianite phase (33°) (Fig. 3). No change in the X-ray diffraction patterns was observed over a period of 10 h of inert treatment for the reduced Co/CeO_2 catalyst at 450 °C. It should be noted that the temperature chosen for inert treatment for the catalyst (450 °C) was higher than the temperature where re-oxidation of cobalt was observed under reaction conditions (300 °C) to promote re-oxidation phenomenon arising from the mobility of oxygen species. Although partial re-oxidation of cobalt species was observed within one hour of the introduction of ESR feed to the reaction chamber, the experiment *involving* inert treatment for a pre-reduced Co/CeO_2 catalyst did not show formation of oxidized cobalt species over a period of 10 h. These results suggest that, during reaction at 300 °C, the re-oxidation of metallic cobalt was caused primarily by dissociative adsorption of water from the gas phase. It should be noted that this result does not rule out the possibility of oxygen diffusion from the support. In fact, our previous work has shown oxygen from ceria to be readily accessible [26]. It is possible that there may have been some oxygen replenishment from the ceria support, but the extent of re-oxidation may have been insufficient to provide any long-range order for an oxide phase to be detected by the XRD technique.

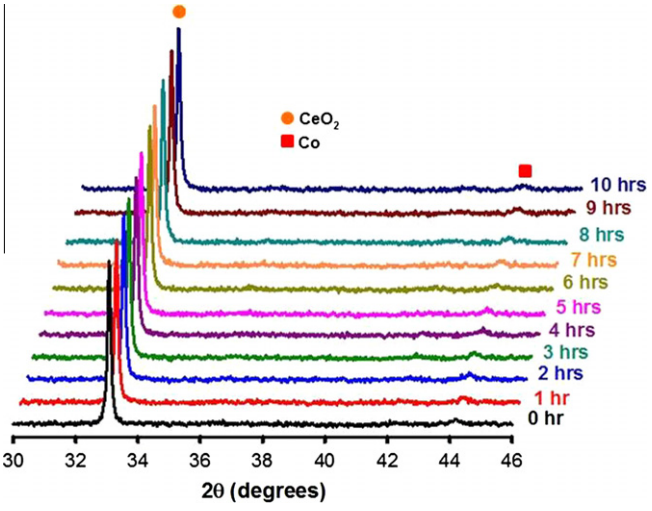

Fig. 3. In situ XRD patterns of Co/CeO_2(R) collected as function of time-on-stream in an inert atmosphere at 400 °C.

Fig. 4 shows the in situ XRD patterns collected during a similar ethanol steam reforming experiment over Co/CeO_2(O). The XRD pattern of the pristine catalyst, which shows cerianite (33°) and Co_3O_4 (31° and 37°), is included in the Figure for comparison. In agreement with the in situ XRD study over Co/CeO_2(R), no change in the cerianite phase was observed at any of the reaction temperatures. Following 30 min of ethanol steam reforming at 300 °C, cobalt oxide (Co_3O_4) was observed to be the only cobalt phase present in the in situ XRD pattern. Upon increasing the reaction temperature to 350 °C, disappearance of diffraction peaks associated with Co_3O_4 and formation of CoO through peaks located at 36.5° and 42.4° were observed. The CoO phase was stable during ethanol steam reforming up to 500 °C. Following 30 min of ethanol steam reforming at 500 °C, a weakly resolved diffraction peak (44°) associated with metallic Co was observed, suggesting further reduction of cobalt oxide species to metallic cobalt at this temperature under the reaction conditions. At 500 °C, both CoO and metallic Co phases were present.

The progression of the reduction of cobalt species from Co_3O_4 to metallic cobalt during ethanol steam reforming was further investigated by keeping the catalyst under ethanol steam reforming feed stream at 500 °C while monitoring the transformation of cobalt phases by in situ XRD. Fig. 5 shows the XRD patterns collected as a function of time-on-stream during this experiment. Within the first hour of reaction, disappearance of the diffraction peaks associated with the Co_3O_4 phase of the pristine catalyst (31° and 37°) and appearance of peaks associated with CoO (36.5° and 42.4°) and metallic Co (44°) was observed. Although weakly resolved after 30 min on stream (see Fig. 3), the peak associated with metallic cobalt phase was well-resolved after an hour on stream. The inset to Fig. 5 shows a comparison of the intensities of peaks associated with CoO (42.4°) and metallic Co (44°) after one hour and 12 h on stream. Comparison of the peak intensities clearly shows a decrease in the intensity of the CoO peak and a concomitant increase in the metallic Co peak, which suggests an increase in the extent of reduction of cobalt species with time-on-stream during ethanol steam reforming under these conditions.

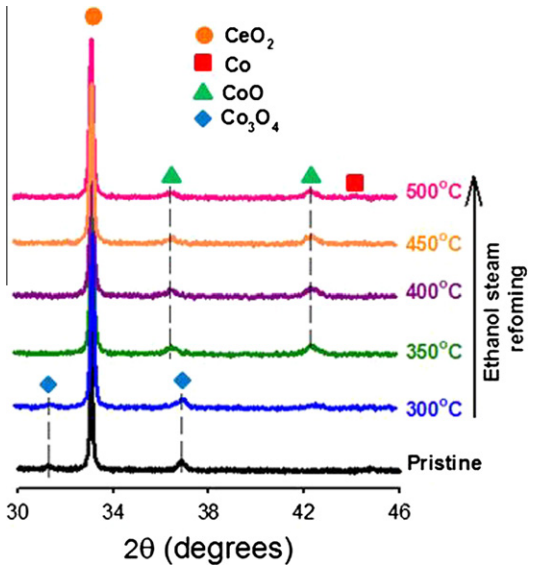

Fig. 4. In situ XRD patterns collected as a function of temperature during ethanol steam reforming over $Co/CeO_2(O)$.

3.3. X-ray absorption spectroscopy (XAFS)

The transformation of cobalt coordination environment during ethanol steam reforming over Co/CeO_2 catalysts that underwent different pretreatments was investigated using X-ray absorption fine structure spectroscopy. Controlled-atmosphere XAFS data were collected at the Co K-edge (7709 eV) at room temperature under helium over $Co/CeO_2(O)$ and $Co/CeO_2(R)$ following catalyst pretreatment and subsequent ethanol steam reforming over the catalysts in the 350–500 °C range. Fig. 6 presents the Co K-edge X-ray absorption near-edge spectra (XANES) collected over $Co/CeO_2(R)$ following ESR over this catalyst together with the XANES spectra of the reference compounds, i.e., CoO and Co, used in linear combination fitting of the XANES region. Also included in Fig. 6 is

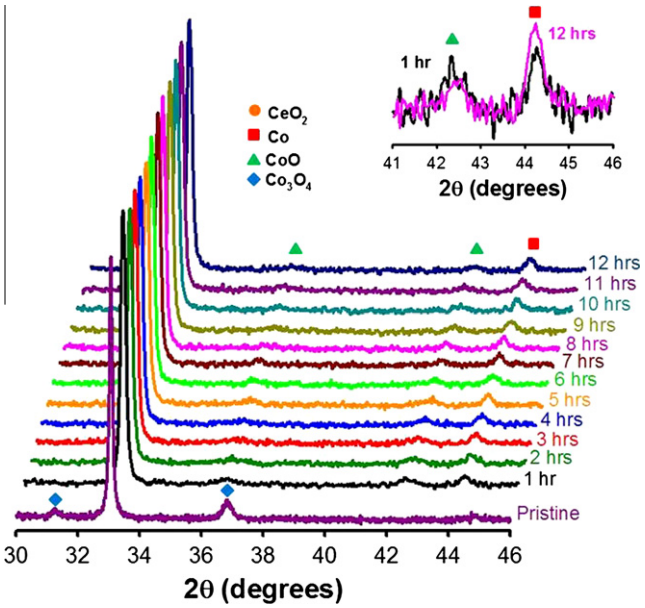

Fig. 5. In situ XRD patterns collected as function of time-on-stream during ethanol steam reforming over $Co/CeO_2(O)$ at 500 °C. (Inset shows a comparison of patterns after 1 h and 12 h onstream.)

the linear combination XANES fitting results to estimate the relative contribution of each cobalt state. Following the reduction pretreatment step, CoO and metallic cobalt were observed to coexist over the catalyst with metallic Co component having a larger contribution. In-line with the in situ XRD results, re-oxidation of some portion of metallic cobalt species to CoO was observed during ethanol steam reforming at 350 °C and the XANES analysis showed a larger fraction of CoO. Although the XRD patterns showed the presence of Co^0 and CoO as the only crystalline phases over pre-reduced Co/CeO_2 and $Co/CeO_2(R)$ after ESR, respectively, the XANES results showing the presence of more than one cobalt phase in each case are not contradictory with the XRD results. Both of the techniques indicate the same major cobalt phase, Co^0 for pre-reduced Co/CeO_2 and CoO for $CO/CeO_2(R)$ after reaction at 350 °C, and XRD technique has lower resolution. Further increase in the reaction temperature resulted in a gradual reduction in CoO to metallic cobalt moieties.

Fig. 7 presents the Co K-edge XANES spectra collected during a similar experiment over $Co/CeO_2(O)$ together with linear combination fitting of the collected spectra with reference compounds. The XANES region of the oxidation-pretreated Co/CeO_2 catalyst was fitted by Co_3O_4 only. With the introduction of reaction feed at 350 °C, the reduction Co_3O_4 species on the $Co/CeO_2(O)$ catalyst was observed and at 400 °C, all Co_3O_4 was completely converted to CoO. Further increase in the reaction temperature led to further reduction in CoO to metallic Co. Such a reduction scheme is in agreement with the previously reported two-step reduction process for unsupported Co_3O_4 and supported cobalt catalysts where Co_3O_4 is converted to CoO, before reduction of CoO to Co^0 takes place [20,22,27,37]. Below 500 °C, the extent of cobalt reduction over the $Co/CeO_2(O)$ catalyst was lower than $Co/CeO_2(R)$; however, the contributions from CoO and Co^0 phases for both $Co/CeO_2(O)$ and $Co/CeO_2(R)$ were, within experimental error, similar after reaction at 500 °C. This observation indicates that same extent of reduction in cobalt species over the Co/CeO_2 catalysts is achieved under reaction conditions regardless of the initial state of cobalt. These results are in agreement with literature [21,38] and clearly show that reduction/oxidation of cobalt species over ceria can take place under these reaction conditions.

The magnitude of k^2-weighted Fourier transforms of the Co K-edge EXAFS spectra collected over the $Co/CeO_2(R)$ catalyst following ESR at the designated temperatures is given in Fig. 8a. Following ESR over the Co/CeO_2 at 350 °C, the Co—Co coordination region in the EXAFS shows a peak at 2.5 Å (peak at 2.14 Å in the uncorrected FT) with a shoulder in the high R region (at c.a. 2.5 Å in the uncorrected FT). The former peak is consistent with Co—Co coordination in metallic Co and the latter is due to scattering from bridging Co—O—Co atoms in CoO environment. The EXAFS spectrum collected following ESR at 400 °C over the same catalyst showed similar features. Above 400 °C, a single Co—Co coordination peak at 2.5 Å, which is consistent with Co^0, was observed. The contributions of Co—O—Co and Co—Co shells to the EXAFS were evaluated by the isolation of the respective coordination shell from the inverse Fourier transform. The reference compounds, CoO and Co-foil, were analyzed by the same procedure. The coordination parameters obtained through fitting the EXAFS data for $Co/CeO_2(R)$ are given in Tables 1. As suggested by the XANES data, cobalt atoms exist in the form of both Co^0 and CoO; therefore, the true coordination numbers were calculated by the fit value of coordination number divided by the fraction of the particular component. The coordination parameters suggest the presence of large cobalt particles over this catalyst.

Fig. 8b shows the magnitude of k^2-weighted Fourier transforms of the Co K-edge EXAFS spectra of $Co/CeO_2(O)$ catalyst following ESR reaction in the 350–500 °C range. Following ESR at 350 °C, the magnitude of the Fourier transform shows a peak at about

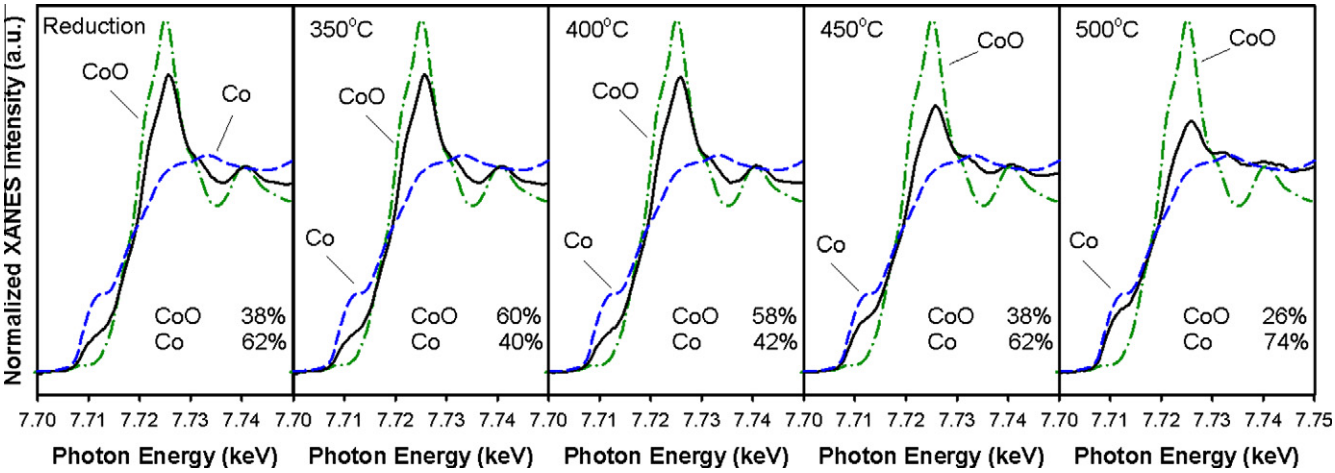

Fig. 6. Normalized XANES spectra and results of linear combination XANES fitting with reference compounds of $Co/CeO_2(R)$ following ethanol steam reforming in the 350–500 °C range.

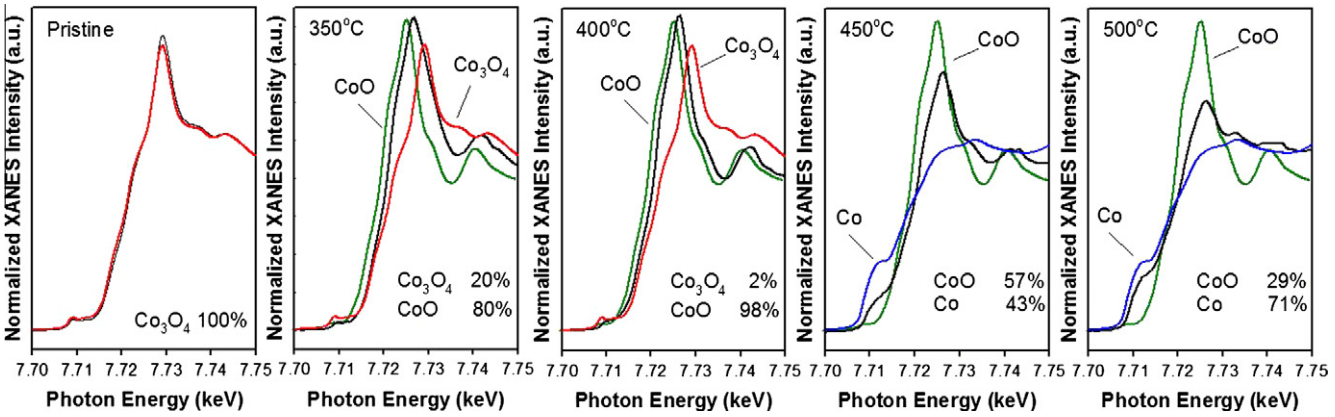

Fig. 7. Normalized XANES spectra and results of linear combination XANES fitting with reference compounds of $Co/CeO_2(O)$ following ethanol steam reforming in the 350–500 °C range.

1.5 Å due to Co—O and another peak at about 2.5 Å due to scattering from bridging Co—O—Co atoms at 3.0 Å. Increasing reaction temperature gives another peak at 2.14 Å, and the peak arising from Co—O scatter from CoO was observed to disappear. This observation is in good agreement with the XRD results indicating the reduction of CoO to metallic cobalt with reaction above 400 °C. The coordination parameters, obtained through isolation of the respective coordination shells, are given in Table 2. These parameters are also in-line with large cobalt particles in each stage of reaction.

3.4. X-ray photoelectron spectroscopy

Fig. 9 shows the X-ray photoelectron spectra in the Co 2p region for pristine Co/CeO_2 and a $Co/CeO_2(O)$ sample that went through the ethanol reaction in the 350–500 °C range. The sample was transferred to the XPS analysis chamber without exposure to air using a special controlled-atmosphere transfer arm. For direct comparability of results from this XPS experiment with the XAFS results, the post-reaction catalyst sample was taken through the same reaction steps as in the XAFS experiment prior to the collection of the XPS spectrum.

The curve fitting of the X-ray photoelectron spectrum of the Co $2p_{3/2}$ region of the pristine catalyst suggests that this envelope is composed of two components located at 779.3 eV and 781.1 eV. In agreement with the assignments in the literature [21,39], the lower binding energy component is assigned to Co^{3+}, while the higher binding energy component was assigned to Co^{2+}. The assignments were further verified by calculating the ratio of the areas under the fitted components. The area ratio of the lower binding energy component to the higher binding energy component was calculated to be ~2, which is consistent with the stoichiometry of Co^{3+} and Co^{2+} species in Co_3O_4.

Over the post-reaction $Co/CeO_2(O)$ catalyst, curve fitting in the Co $2p_{3/2}$ region suggested the presence of three features assigned to Co^0 (779 eV), Co^{2+} (781.4 eV) and a shake-up component associated with paramagnetic Co^{2+} species and is displaced by 4.1 eV relative to the Co^{2+} main photopeak. The relative contributions of the Co^0 and Co^{2+} components to the main photopeak were calculated from the areas under the curve for the respective components as 70% and 30%, respectively. These values are in agreement with the XANES results and show that the average oxidation state of the cobalt surface species closely resembles that of the bulk.

3.5. Steady state catalytic activity testing

Steady state activity testing was carried out over $Co/CeO_2(O)$ and $Co/CeO_2(R)$ to investigate the effect of catalyst pretreatment on the ESR activity and to correlate the transformation of cobalt phases observed through the in situ XRD and XAFS experiments with the catalytic activity of Co/CeO_2 catalysts in ethanol steam reforming reaction. Fig. 10 compares the H_2 production rates

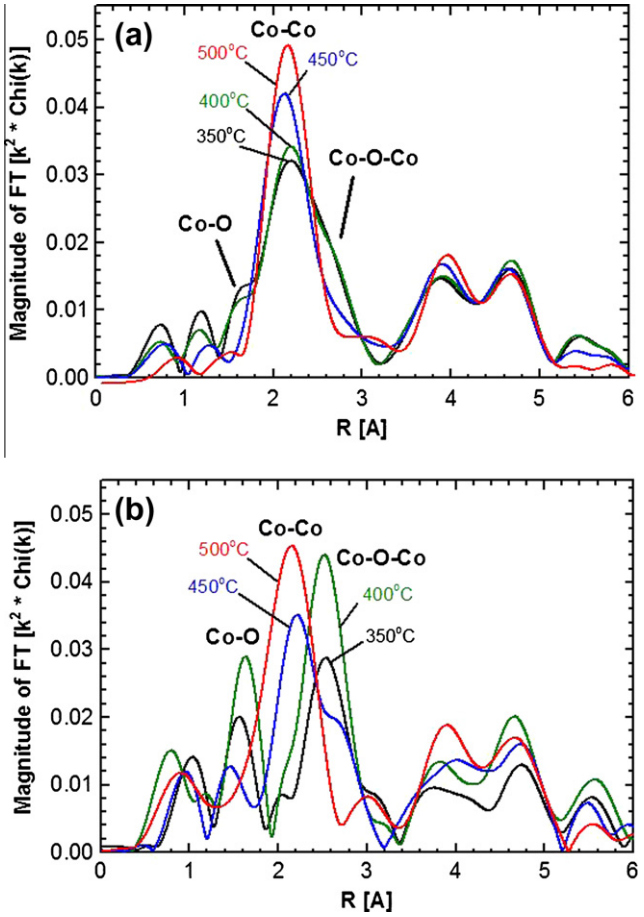

Fig. 8. Magnitude of k^2-weighted Fourier transforms of cobalt K-edge EXAFS spectra collected following ethanol steam reforming in the 350–500 °C range over (a) $Co/CeO_2(R)$ and (b) $Co/CeO_2(O)$.

Table 1
Results of EXAFS fitting of $Co/CeO_2(R)$ at the Co K-edge.

Temperature	Scatter	CN	CN fit	R (Å)	$\Delta\sigma$ (Å^2)	ΔE_0 (eV)
350 °C	Co—Co	11.7	4.7	2.50	0.0010	−1.70
	Co—O—Co	10.1	6.1	3.00	0.0005	−0.87
400 °C	Co—Co	11.9	5.0	2.50	0.0010	−1.68
	Co—O—Co	11.9	6.9	2.99	0.0010	−1.28
450 °C	Co—Co	11.9	7.4	2.50	0.0007	−1.45
	Co—O—Co	12.0	4.6	3.01	0.0010	−0.57
500 °C	Co—Co	11.8	8.7	2.50	0.0005	−1.45

Table 2
Results of EXAFS fitting of $Co/CeO_2(O)$ at the Co K-edge.

Temperature	Scatter	CN	CN fit	R (Å)	$\Delta\sigma$ (Å^2)	ΔE_0 (eV)
350 °C	Co—O—Co	10.2	8.2	3.00	0.0010	1.02
400 °C	Co—O—Co	11.9	11.9	3.00	0.0005	−0.06
450 °C	Co—Co	10.9	4.7	2.46	0.0010	−5.91
	Co—O—Co	11.9	6.8	3.02	0.0005	0.52
500 °C	Co—Co	11.9	8.4	2.49	0.0006	−2.11

(TOF) over $Co/CeO_2(O)$ and $Co/CeO_2(R)$. In the same figure, the inset shows the Arrhenius plots obtained using the TOFs calculated for the two catalysts, as described in Section 2.3. The production rates of carbon-containing products of ethanol steam reforming are presented in Table 3. Below 450 °C, $Co/CeO_2(O)$ achieved significantly lower H_2 and CO_2 production rates than $Co/CeO_2(R)$; however, as

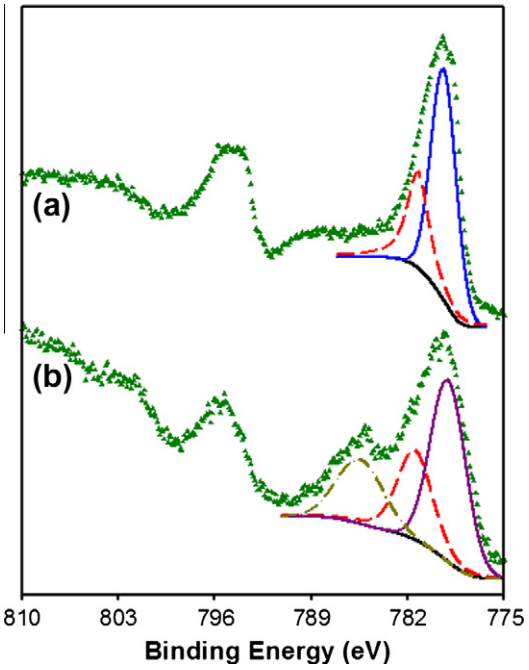

Fig. 9. X-ray photoelectron spectra of (a) Co/CeO_2 (pristine), (b) $Co/CeO_2(O)$ following ethanol steam reforming in the 350–500 °C range.

the reaction temperature is increased, $Co/CeO_2(O)$ catalyst was activated rapidly and was capable of achieving rates similar to its pre-reduced counterpart (see Fig. 10). This behavior is consistent with the XRD and XAFS results where the transformation of cobalt phases under ethanol steam reforming conditions was observed to yield the same composition of CoO and metallic Co phases, regardless of the initial state of cobalt on the catalyst. It seems that both CoO and Co^0 exist over the catalyst showing high activity. Furthermore, the $Co/CeO_2(O)$ catalyst which was shown to consist of CoO mainly at 400 °C through the analysis of the XANES data (See Fig. 7) is not capable of achieving similar production rates for H_2 and CO_2 as $Co/CeO_2(R)$, indicating that the presence of CoO alone is not enough for achieving high steam reforming activity, although Co^{2+} sites appear to have some intrinsic activity themselves. The takeoff of the steam reforming reaction over the oxidation-pretreated catalyst was observed only after cobalt species with metallic character formed over the surface, suggesting the importance of coexistence of CoO and Co phases for achieving high steam reforming activity. Previously, Llorca et al. [19] have reported similar conclusions on the presence of an equilibrium state between CoO and Co^0 over supported cobalt catalysts during ethanol steam reforming, and Lin et al. [21] showed that such an equilibrium state between CoO and metallic Co is influenced by the water-to-ethanol ratio in the feed. The activation energies obtained using the Arrhenius plots shown in the inset are 26 and 112 kJ/mole for the $Co/CeO_2(R)$ and $Co/CeO_2(O)$ catalysts, respectively. It should be noted that these are apparent activation energies and do not take into account the changing nature of the degree of reduction in the catalyst with temperature.

TOFs for the Co^0 and Co^{2+} sites were also calculated using the XANES data to obtain the number of Co^0 and Co^{2+} sites. The calculation procedure is outlined in Section 2.3. It should be noted that these calculations involve some assumptions. For example, at each temperature, it is assumed that each of the Co^0 sites has the same TOF, regardless of the catalyst matrix they belong to. A similar assumption is made for the Co^{2+} sites. This is a simplifying assumption, and in reality, one would expect that the coordination environment of each site (i.e., whether it is neighboring more of the

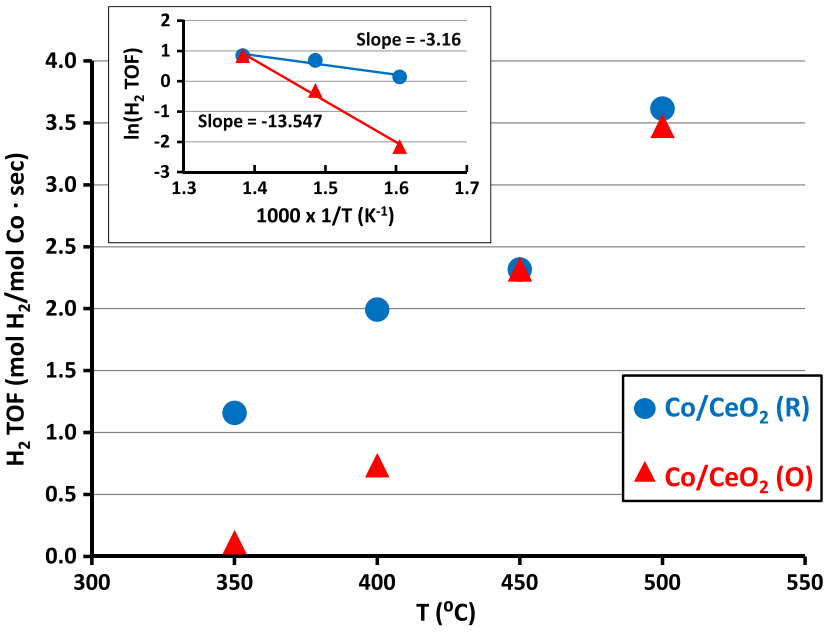

Fig. 10. Effect of oxidation (triangles) and reduction (circles) pretreatment on H_2 production rate as a function of temperature over Co/CeO_2. WHSV = 2.7 g EtOH (g cat)$^{-1}$ h^{-1}, C_{EtOH} = 0.8% and H_2O:EtOH = 10:1 (molar ratio). (Inset shows the Arrhenius plots obtained using TOFs based on total surface Co atoms).

Table 3
Effect of pretreatment conditions on the production rates of carbon-containing products of ESR [1000 × (mol (mol of Co)$^{-1}$ s^{-1})] WHSV = 2.7 g EtOH (g cat)$^{-1}$ h^{-1}, C_{EtOH} = 0.8% and H_2O:EtOH = 10:1 (molar ratio).

Products	350 °C		400 °C		450 °C		500 °C	
	(O)	(R)	(O)	(R)	(O)	(R)	(O)	(R)
CO	0.6	2.7	2.1	3.3	5.0	4.7	9.9	10.5
CH_4	–	–	0.1	0.1	0.2	0.1	0.2	0.0
C_2H_4	0.1	0.1	0.5	0.2	0.5	0.2	0.9	0.7
C_2H_6	–	–	0.1	0.1	0.1	0.3	–	0.1
CH_3COCH_3	0.6	0.2	0.6	0.9	0.9	1.0	1.3	1.4
CH_3CHO	0.4	0.6	1.4	1.2	1.0	1.6	1.6	1.9

metallic sites or oxide sites) would change its activity. Another assumption involved in the calculations is that the compositions obtained from XANES, which is a bulk technique, are representative of the surface compositions. The fact that the XPS data obtained from a post-reaction $Co/CeO_2(O)$ catalyst that went through the 350–500 °C reaction sequence gave compositions not too different from the XANES data may be used to justify this assumption. However, there may be differences in the abundance of the metallic and oxidic sites on the surface versus in the bulk. Finally, including only two type of sites, i.e., of Co^0 and Co^{2+}, may also be an oversimplification. For example, there is evidence that metallic sites supported on reducible oxides such as ceria may undergo electron transfer with the support and may assume positive charges ($Co^{\delta+}$) [40,41]. The TOFs calculated for the Co^0 and Co^{2+} sites are plotted as a function of temperature in Fig. 11. The TOFs for the Co^0 sites change from 2.4 to 4.2 s^{-1} in the 350–500 °C temperature range. These TOFs are comparable to those reported for transition metals, e.g., (2.2–10 s^{-1} for Ni/MgO catalysts at 650 °C[42], ~0.1 s^{-1} for Cu—Ni catalysts at 550 °C[43]), or even for precious metals (1–20 s^{-1} for Rh/MgO at 650 °C[44]). The TOFs for the Co^{2+} sites vary from 0.2 to 1.7 s^{-1} in the same temperature range. As expected, the intrinsic activity of metallic sites is much higher than that of the Co^{2+} sites. The Arrhenius plots constructed using the TOFs for individual sites are presented in the inset of Fig. 11. The activation energies calculated from these plots for the Co^0 and Co^{2+} sites are 15 and 67 kJ/mol, respectively.

Throughout the temperature range, CO_2, CO, CH_4, C_2H_6 and liquid by-products such as acetaldehyde and acetone were also observed in varying quantities in addition to H_2. Ethanol steam reforming reaction network over Co-based catalysts is governed by a large number of intermediate steps and side reactions. A comparison of the production rates of carbon-containing species over $Co/CeO_2(O)$ and $Co/CeO_2(R)$ is given in Table 3. As expected, CO_2 is the main carbon-containing product over $Co/CeO_2(R)$ at all temperatures. Over $Co/CeO_2(O)$, the CO_2 production rate slowly increases with temperature, reaching the same level with the pre-reduced catalyst at 450 °C. Acetaldehyde, which is a product of ethanol dehydrogenation and an intermediate of ethanol steam reforming over cobalt-based catalysts, was observed over both $Co/CeO_2(O)$ and $Co/CeO_2(R)$. In the literature, both CoO [18] and Co_3O_4 [20,22,36] have been reported to exhibit activity for selective dehydrogenation ethanol to yield acetaldehyde. Acetone, produced through aldol condensation of acetaldehyde, was observed as one of the two liquid by-products at all temperatures. The high acetone production rates observed over the $Co/CeO_2(O)$ catalyst at 350 °C suggest a propensity for the oxide phases for aldol condensation-type reactions since this catalyst does not have any metallic sites at this temperatures. One of the reason for the higher rates observed for the liquid by-products is the high WHSVs used in these experiments to keep the conversion levels low. Similar observations on the product distribution over a similar Co/CeO_2 catalyst have previously been reported by Song and Ozkan [27].

Ethane, methane, and CO are the other products produced in small quantities, with CO giving the lowest yields. Despite the differences in product distribution at lower temperatures, above 400 °C, the rates of formation of all the reaction products were very similar within experimental error. This observation is in agreement with the catalyst characterization studies aiming at identifying the state of cobalt under reaction conditions. The differences in the state of cobalt tend to diminish under reaction conditions with increasing temperature, which is fully aligned with the observed rates of the reaction products that converge to similar values as reduction in cobalt to the metallic form takes place during reaction. It should be noted that the ethanol steam reforming reaction is governed by a complex network of reactions, as reported previ-

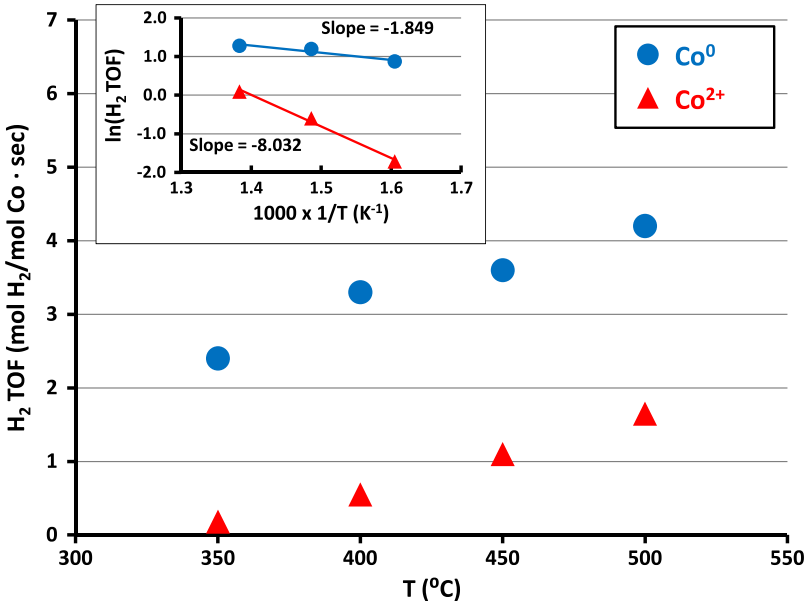

Fig. 11. Change of TOFs with temperature for Co^0 and Co^{2+} species based on XANES data. Inset: Arrhenius plots obtained using the TOFs.

ously [45,46], but there was no attempt at elucidating the complexities of the reaction network in this study.

3.6. In situ DRIFTS during ethanol steam reforming

The effect of pretreatment on the evolution of surface intermediates during steam reforming of ethanol over Co/CeO_2 was further investigated using DRIFTS. In situ DRIFT spectra were collected, while ethanol steam reforming reaction is progressing over the catalyst and after flushing reactants from the DRIFTS chamber with helium. Figs. 12a and 13a present the in situ DRIFT spectra collected as a function of temperature in the 25–500 °C range during such experiments over Co/CeO_2(O) and Co/CeO_2(R), respectively. Figs. 12b and 13b show the spectra after the DRIFTS chamber was flushed with He. Over Co/CeO_2(R), the formation of a broad band is observed in the 3600–3200 cm^{-1} region was observed upon introduction of the ethanol steam reforming reaction feed to the in situ DRIFTS chamber (Fig. 9). This peak was observed to decrease in intensity with increasing temperature, disappearing completely at 200 °C. This band is associated with surface hydroxyls and adsorbed water on the surface. In the low wavenumber region, another weakly resolved feature was observed around 1650 cm^{-1}, which disappears above 100 °C. This peak is associated with molecularly adsorbed water [47]. A similar control experiment was performed over the same sample, where ethanol was eliminated from the feed stream and only water vapor was fed to the reaction chamber (data not shown). During this experiment, the 1650 cm^{-1} feature was observed to exhibit the same behavior as in the in situ DRIFTS ethanol steam reforming temperature-programmed reaction experiment. It should be noted that water vapor was being fed to the DRIFTS controlled-atmosphere chamber during the collection of the spectra presented in Figs. 12a and 13a and therefore, bands arising from the rotational modes of the water molecule in the gas phase are observed in the 3600–3500 cm^{-1} and 1800–1300 cm^{-1} regions. A significant decrease in the intensity of these bands, as presented in Figs. 12b and 13b was observed upon flushing the chamber with helium.

Along with the aforementioned absorption bands arising from the interaction of water vapor with the catalyst surface, several other bands at 2964, 2931, 1049, and 844 cm^{-1} were observed at 25 °C under the ethanol steam reforming reaction feed. These bands arise from interaction of ethanol with the catalyst surface and have been associated with ν_{as} (CH_3) at 2964 cm^{-1}, ν_s (CH_3) at 2931 cm^{-1}, ν (CO) at 1049 cm^{-1}, and ν (COO) at 844 cm^{-1} modes of surface ethoxy species. Formation of ethoxy species is indicative of associative adsorption of ethanol onto the catalyst, yielding surface ethoxy and hydroxy species [12,47–51]. Ethoxy species were not stable during helium flush (Fig. 12b). Over Co/CeO_2(R), the intensity of the ethoxy species decreased with increasing temperature (see Fig. 12a). Above 100 °C, concomitant appearance of absorption bands at 1577 cm^{-1} and 1465 cm^{-1} in the C=O vibration fingerprint region was observed. Especially at 100 °C, these bands are not readily observed in the spectrum collected during in situ reaction due to the presence of bands in the C=O fingerprint region arising from the presence of water vapor. However, flushing the chamber with helium allows for better resolution in this region (see Fig. 12b). These bands are associated with asymmetric and symmetric vibrations of acetate species, respectively [3–6]. It is also possible to associate 1537 cm^{-1} band with ν_{asymm}(COO) vibrations of carbonate or formate species. Formation of these species suggests the conversion of ethoxy species to surface acetate and possibly carbonate species with increasing temperature. Along with the disappearance of ethoxy species and formation of acetate species at 100 °C, formation of CO_2 (2354 cm^{-1} and 2323 cm^{-1}) was also observed signaling the kickoff of ethanol steam reforming reaction. Above 250 °C, acetate species were not stable after helium flush.

The transformation of ethoxide species to acetate has been associated with the presence of CoO moieties on the surface that produce acetaldehyde through dehydrogenation [18], and acetaldehyde was further oxidized to acetate species on the surface [52,53]. The 3014 cm^{-1} band observed in the DRIFT spectrum collected during ethanol steam reforming at 200 °C and then again at 500 °C is the characteristic of methane. Co/CeO_2 catalysts are extensively studied for preferential oxidation of carbon monoxide and have been reported to exhibit methanation activity above 250 °C [54]. In agreement with literature, the low temperature evolution of methane can be associated with methanation reaction although decomposition of acetaldehyde cannot be ruled out. At higher temperatures, on the other hand, ethanol decomposition

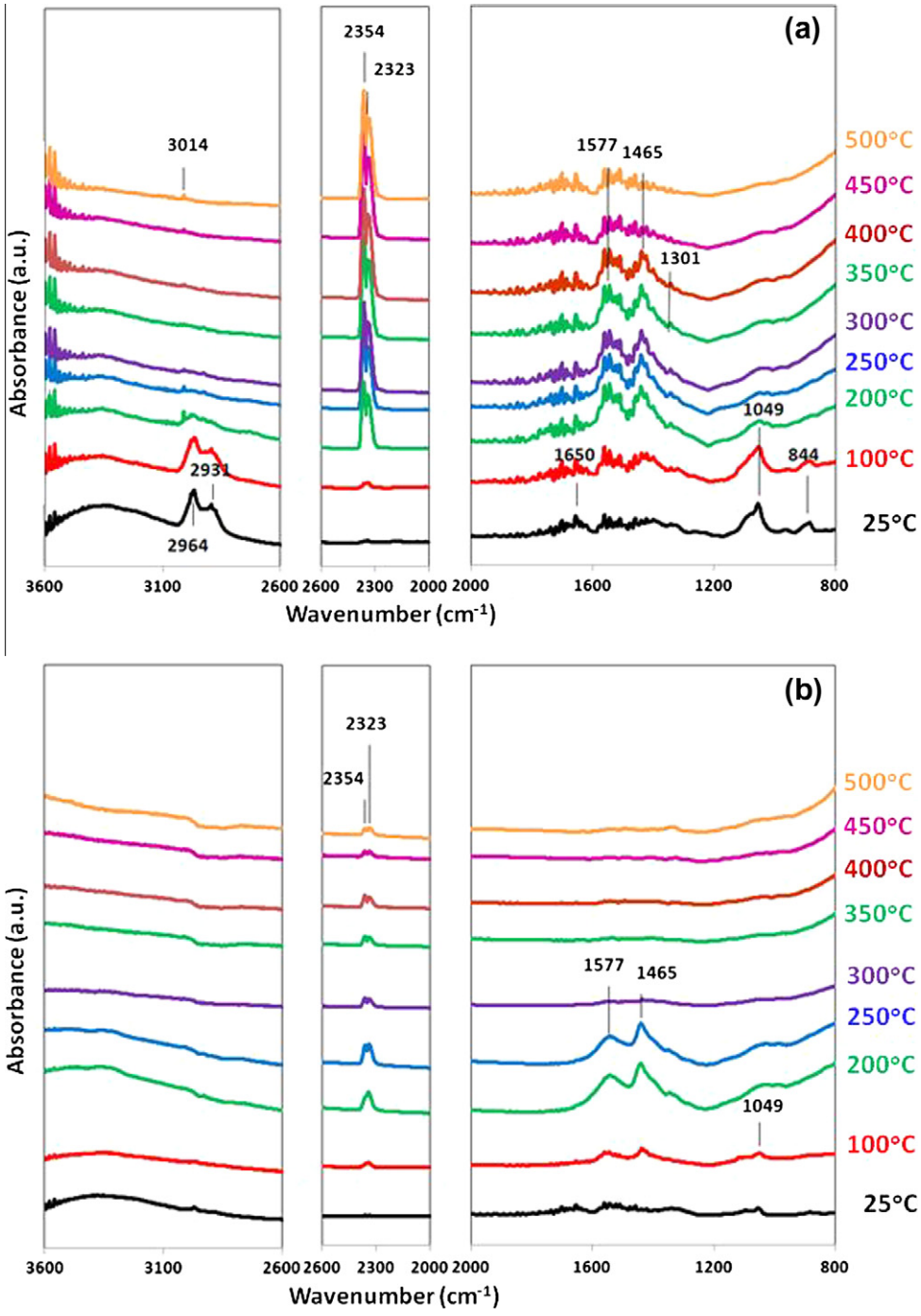

Fig. 12. DRIFT spectra collected as a function of temperature during ethanol steam reforming over $Co/CeO_2(R)$ (a) spectra acquired in situ and (b) spectra acquired after flushing with He.

to yield methane, carbon monoxide, and hydrogen takes off and the methane band observed at higher temperatures was associated with this reaction.

Fig. 13a presents DRIFT spectra collected under reactant flow during a similar ethanol steam reforming temperature-programmed reaction experiment over $Co/CeO_2(O)$ where the formation of similar surface species to $Co/CeO_2(R)$ was observed. Consistent with the foregoing discussion, formation of ethoxy (2964 cm^{-1}, 2931 cm^{-1}, 1049 cm^{-1}, and 844 cm^{-1}) species and hydroxy groups (3600–3200 cm^{-1}) was observed with the introduction of the reaction feed at room temperature. In agreement with the previous discussion on the surface species over $Co/CeO_2(R)$, after flushing the reactant gas mixture from the DRIFTS chamber, formation of surface acetate species was observed at 100 °C (Fig. 13b). Above 200 °C, formation of acetate species was coupled with decrease in the intensity of the ethoxy bands. It is worth noting that although the formation of acetate species was observed at the same temperature over both $Co/CeO_2(O)$ and $Co/CeO_2(R)$, the ethoxy species persisted until higher temperatures over the $Co/CeO_2(O)$ while complete disappearance of the ethoxy bands was observed at 250 °C over $Co/CeO_2(R)$. This observation is in agreement with the steady state activity tests, where lower rates of acetaldehyde formation were observed over the oxidation-pretreated catalyst (see Table 3). Similar observations on the stability of eth-

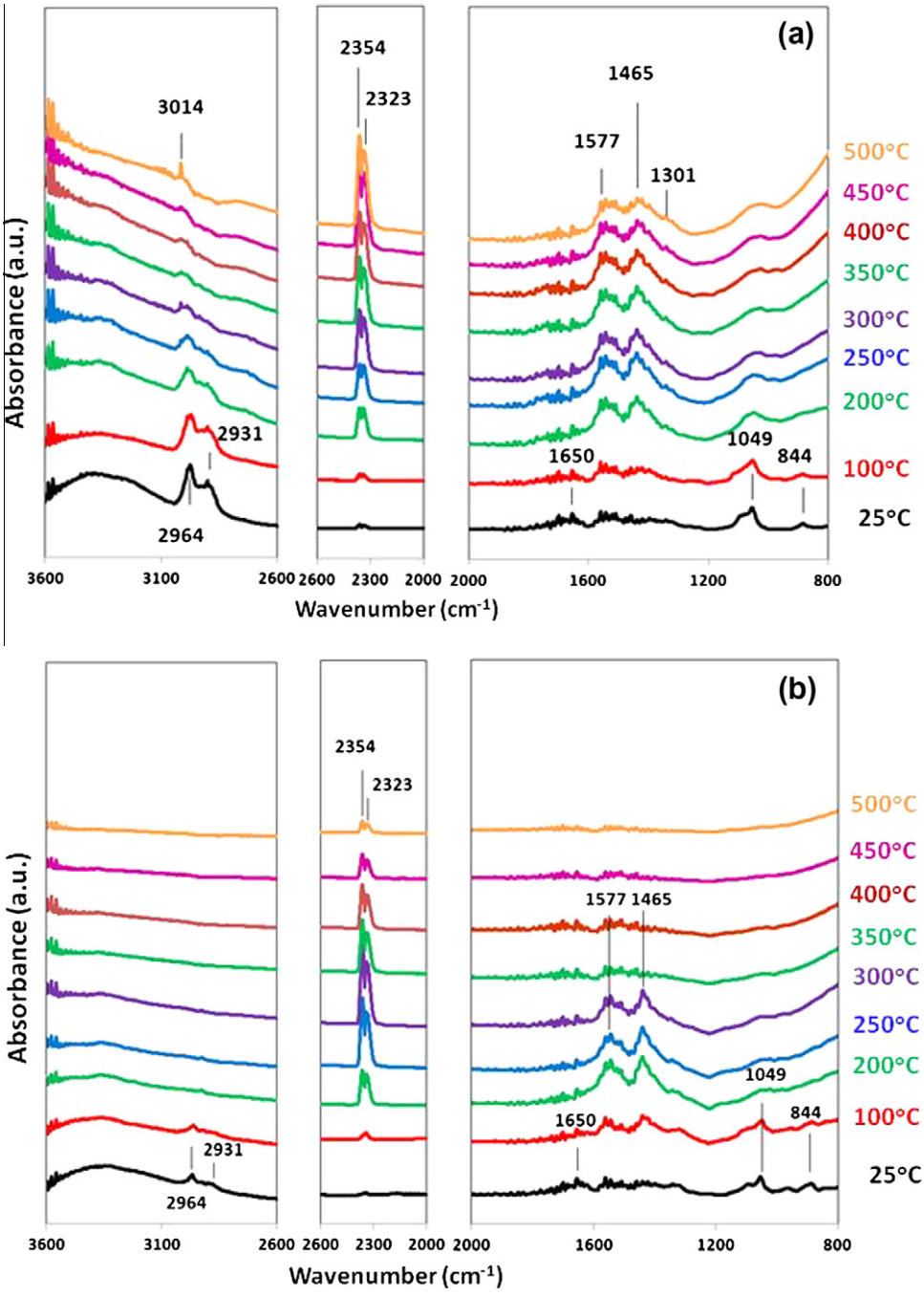

Fig. 13. DRIFT spectra collected as a function of temperature during ethanol steam reforming over $Co/CeO_2(O)$ (a) spectra acquired in situ and (b) spectra acquired after flushing with He.

oxy species on Co_3O_4 were also reported by Hyman and Vohs [18]. Similarly, formation of CO_2 (2354 cm^{-1} and 2323 cm^{-1}), which signals the onset of steam reforming reaction, was observed at 200 °C over both $Co/CeO_2(O)$ and $Co/CeO_2(R)$; however, the intensity of the CO_2 bands was significantly lower over $Co/CeO_2(O)$. These observations suggest that conversion of adsorbed ethoxy species on the pre-reduced Co/CeO_2 catalyst proceeds at a faster rate than its pre-oxidized counterpart. As the temperature is increased, the intensity of CO_2 bands increase over $Co/CeO_2(O)$, indicating the takeoff of steam reforming reaction. The DRIFTS results are aligned with the steady state activity evaluation, and in situ characterization results discussed above and show that similar reaction intermediates are formed on the catalyst surface. However, the transformation of surface intermediates to reaction products is shifted to higher temperatures over $Co/CeO_2(O)$ compared to its pre-reduced counterpart.

4. Conclusions

In situ X-ray diffraction and controlled-atmosphere X-ray absorption and X-ray photoelectron spectroscopy studies together with steady state activity measurements were used to examine the transformation of cobalt species during ethanol steam reforming and to correlate the catalytic activity with the observed cobalt phases. The effect of the initial state of cobalt on the steady state

catalytic activity and the state of cobalt over the Co/CeO_2 catalyst under reaction conditions was investigated by pretreating the catalyst under an oxidizing or a reducing atmosphere. The catalyst that underwent an oxidation pretreatment was initially comprised of Co_3O_4 and went through a gradual reduction under reaction conditions. The reduction in Co_3O_4 species coincided with the activation the oxidized catalyst. Similarly, partial re-oxidation of metallic cobalt over the catalyst that was pretreated with reduction took place under reaction medium at lower temperatures. Regardless of the initial state of cobalt, coexistence of CoO and metallic Co in similar proportions was observed over both of the catalysts when a reaction temperature of 450 °C was reached. While Co_3O_4 was inactive for steam reforming of ethanol, the active catalyst had both CoO and Co^0 species. It is possible that depending on the feed conditions, the phase composition of the catalysts at steady state may converge at different temperatures. The DRIFTS results were in good agreement with the characterization and steady state reaction results showing that reduction of Co_3O_4 was necessary for further conversion of ethoxy species.

Acknowledgments

We gratefully acknowledge the funding from the US Department of Energy through the Grant DE-FG36-05GO15033. Portions of this work were performed at the DuPont-Northwestern-Dow Collaborative Access Team (DND-CAT) located at Sector 5 of the Advanced Photon Source (APS). DND-CAT is supported by E.I. DuPont de Nemours & Co., The Dow Chemical Company and the State of Illinois. Use of the APS was supported by the US Department of Energy, Office of Science, Office of Basic Energy Sciences, under Contract No. DE-AC02-06CH11357.

Appendix A. Supplementary material

Supplementary data associated with this article can be found, in the online version, at doi:10.1016/j.jcat.2011.09.001.

References

[1] L.F. Brown, Int. J. Hydrogen Energy 26 (2001) 381.
[2] A. Bshish, Z. Yakoob, B. Narayanan, R. Ramakrishnan, A. Ebshish, Chem. Pap. 65 (2011) 251.
[3] A. Haryanto, S. Fernando, N. Murali, S. Adhikari, Energy Fuels 19 (2005) 2098.
[4] M. Ni, D.Y.C. Leung, M.K.H. Leung, Int. J. Hydrogen Energy 32 (2007) 3238.
[5] F. Aupretre, C. Descorme, D. Duprez, Catal. Commun. 3 (2002) 263.
[6] P.Y. Sheng, A. Yee, G.A. Bowmaker, H. Idriss, J. Catal. 208 (2002) 393.
[7] A.C.W. Koh, W.K. Leong, L. Chen, T.P. Ang, J. Lin, B.F.G. Johnson, T. Khimyak, Catal. Commun. 9 (2008) 170.
[8] V. Fierro, V. Klouz, O. Akdim, C. Mirodatos, Catal. Today 75 (2002) 141.
[9] H. Idriss, Platinum Metals Rev. 48 (2004) 105.
[10] J.R. Salge, G.A. Deluga, L.D. Schmidt, J. Catal. 235 (2005) 69.
[11] J. Comas, F. Marino, M. Laborde, N. Amadeo, Chem. Eng. J. 98 (2004) 61.
[12] A. Erdohelyi, J. Rasko, T. Keckske, M. Toth, M. Domok, K. Baan, Catal. Today 116 (2006) 367.
[13] J.-L. Bi, Y.-Y. Hong, C.-C. Lee, C.-T. Yeh, C.-B. Wang, Catal. Today 129 (2007) 322.
[14] J.P. Breen, R. Burch, H.M. Coleman, Appl. Catal. B 39 (2002) 65.
[15] P.Y. Sheng, W.W. Chiu, A. Yee, S.J. Morrison, H. Idriss, Catal. Today 129 (2007) 313.
[16] J. Llorca, N. Homs, J. Sales, P.R. de la Piscina, J. Catal. 209 (2002) 306.
[17] H. Song, L. Zhang, R.B. Watson, D. Braden, U.S. Ozkan, Catal. Today 129 (2007) 346.
[18] M.P. Hyman, J.M. Vohs, Surf. Sci. 605 (2011) 383.
[19] J. Llorca, J.-A. Dalmon, P. Ramirez de la Piscina, N. Homs, Appl. Catal. A 243 (2003) 261.
[20] J. Llorca, P.R.d.l. Piscina, J.-A. Dalmon, N. Homs, Chem. Mater. 16 (2004) 3573.
[21] S.S.Y. Lin, D.H. Kim, M.H. Engelhard, S.Y. Ha, J. Catal. 273 (2010) 229.
[22] V.A. de la Pena O'Shea, N. Homs, E. Pereira, R. Nafria, P. Ramirez de la Piscina, Catal. Today 126 (2007) 148.
[23] M.S. Batista, R.K.S. Santos, E.M. Assaf, J.M. Assaf, E.A. Ticianelli, J. Power Sources 124 (2003) 99.
[24] H. Song, B. Mirkelamoglu, U.S. Ozkan, Appl. Catal. A 382 (2010) 58.
[25] H. Song, U.S. Ozkan, J. Catal. 261 (2009) 66.
[26] H. Song, U.S. Ozkan, J. Phys. Chem. A 114 (2010) 3796.
[27] H. Song, U.S. Ozkan, J. Mol. Catal. A 318 (2010) 21.
[28] H. Song, B. Tan, U.S. Ozkan, Catal. Lett. 132 (2009) 422.
[29] J.R. Jensen, T. Johannessen, H. Livbjerg, Appl. Catal. A 266 (2004) 117.
[30] B.R. Fingland, F.H. Ribeiro, J.T. Miller, Catal. Lett. 131 (2009) 1.
[31] J.H. Pazmino, J.T. Miller, S.S. Mulla, W. Nicholas Delgass, F.H. Ribeiro, J. Catal. 282 (2011) 13.
[32] J.T. Miller, W.J. Reagan, J.A. Kaduk, C.L. Marshall, A.J. Kropf, J. Catal. 193 (2000) 123.
[33] T. Ressler, J. Phys. IV 7 (1997) 269.
[34] J.T. Miller, C.L. Marshall, A.J. Kropf, J. Catal. 202 (2001) 89.
[35] H. Song, L. Zhang, U.S. Ozkan, Green Chem. 9 (2007) 686.
[36] S. Tuti, F. Pepe, Catal. Lett. 122 (2008) 196.
[37] G. Jacobs, Y. Ji, B.H. Davis, D. Cronauer, A.J. Kropf, C.L. Marshall, Appl. Catal. A 333 (2007) 177.
[38] S.S.Y. Lin, D.H. Kim, S.Y. Ha, Appl. Catal. A 355 (2009) 69.
[39] L.F. Liotta, G. Di Carlo, G. Pantaleo, A.M. Venezia, G. Deganello, Appl. Catal. B 66 (2006) 217.
[40] J. Rodriguez, P. Liu, J. Hrbek, J. Evans, M. Pérez, Angew. Chem. Int. Ed. 46 (2007) 1329.
[41] J. Hu, W.-P. Guo, X.-R. Shi, B.-R. Li, J. Wang, J. Phys. Chem. C 113 (2009) 7227.
[42] F. Frusteri, S. Freni, V. Chiodo, L. Spadaro, O. Di Blasi, G. Bonura, S. Cavallaro, Appl. Catal. A 270 (2004) 1.
[43] F.J. Marino, E.G. Cerrella, S. Duhalde, M. Jobbagy, M.A. Laborde, Int. J. Hydrogen Energy 23 (1998) 1095.
[44] N. Palmeri, S. Cavallaro, V. Chiodo, S. Freni, F. Frusteri, J.C.J. Bart, Int. J. Hydrogen Energy 32 (2007) 3335.
[45] H. Song, X. Bao, C.M. Hadad, U.S. Ozkan, Catal. Lett. 141 (2011) 43.
[46] H. Song, L. Zhang, U.S. Ozkan, Ind. Eng. Chem. Res. 49 (2010) 8984.
[47] L.V. Mattos, F.B. Noronha, J. Catal. 233 (2005) 453.
[48] J. Llorca, N. Homs, J. Sales, J. Fierro, G. Luis, P. Ramirez de la Piscina, J. Catal. 222 (2004) 470.
[49] J.M. Guil, N. Homs, J. Llorca, P.R. de la piscina, J. Phys. Chem. B 109 (2005) 10813.
[50] J. Rasko, M. Domok, K. Baan, A. Erdohelyi, Appl. Catal. A 299 (2006) 202.
[51] H. Idriss, M. Scott, J. Llorca, S.C. Chan, W. Chiu, P.-Y. Sheng, A. Yee, M.A. Blackford, S.J. Pas, A.J. Hill, F.M. Alamgir, R. Rettew, C. Petersburg, S.D. Senanayake, M.A. Barteau, ChemSusChem 1 (2008) 905.
[52] M. Benito, J.L. Sanz, R. Isabel, R. Padilla, R. Arjona, L. Daza, J. Power Sources 151 (2005) 11.
[53] J. Llorca, N. Homs, P. Ramirez de la Piscina, J. Catal. 227 (2004) 556.
[54] M.P. Woods, P. Gawade, B. Tan, U.S. Ozkan, Appl. Catal. B 97 (2010) 28.